Cell Reports, Volume *31*

Supplemental Information

Structure of Human ATG9A, the Only Transmembrane Protein of the Core Autophagy Machinery

Carlos M. Guardia, Xiao-Feng Tan, Tengfei Lian, Mitra S. Rana, Wenchang Zhou, Eric T. Christenson, Augustus J. Lowry, José D. Faraldo-Gómez, Juan S. Bonifacino, Jiansen Jiang, and Anirban Banerjee

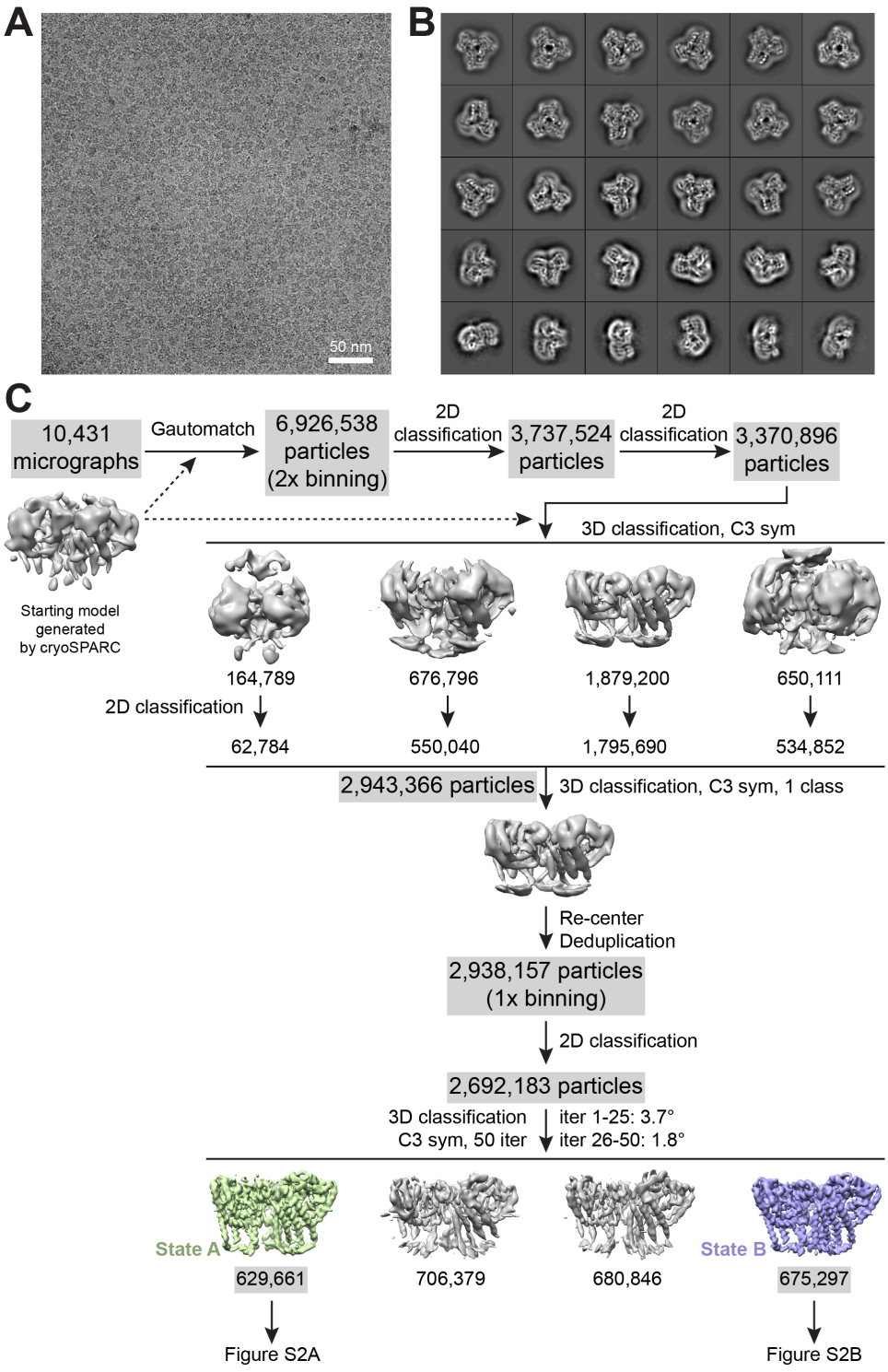

Figure S1. CryoEM data processing of ATG9A in the detergent LMNG, *Related to Figure 1*. (**A**) CryoEM micrograph of the ATG9A sample. (**B**) 2D class averages of ATG9A particles showing the feature of 3-fold symmetry and views at different angles. (**C**) Flowchart of the data processing procedures for 2D classification and 3D classification. Two conformational states (state A and state B) were identified and the particles in these two states were further processed to obtain high-resolution structures (shown in Figure S2).

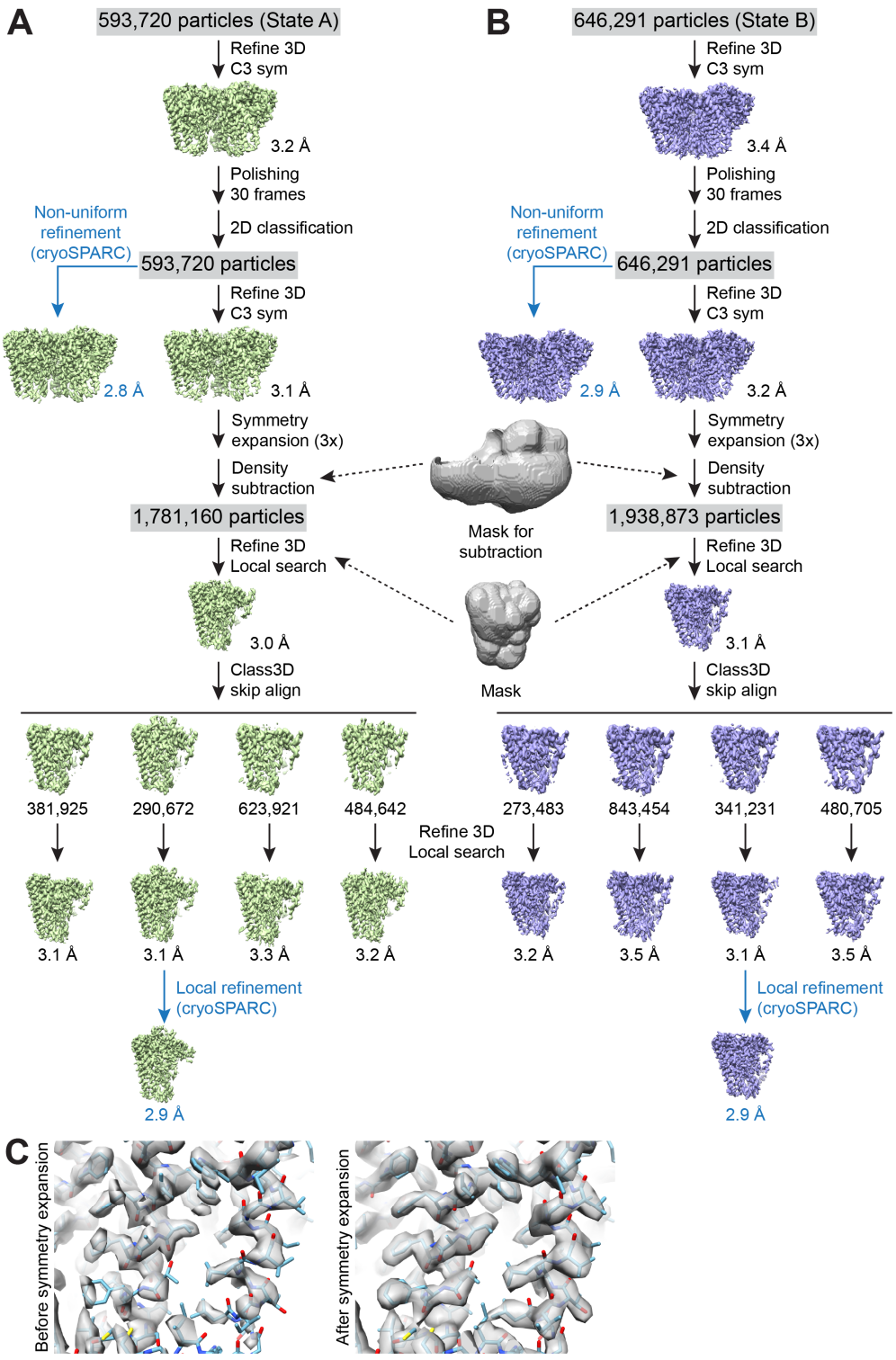

Figure S2. High-resolution 3D reconstruction and refinement of ATG9A, *Related to Figures 1 and 2.* (**A** and **B**) Flowchart of cryoEM 3D refinement with symmetry expansion and density subtraction of states A and B. (**C**) Comparison of the cryoEM density maps before and after the symmetry expansion showing improvement on both resolution and quality.

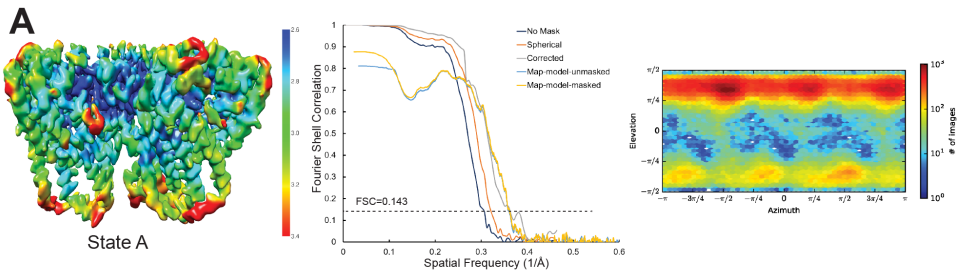
A
State A
No Mask
Spherical
Corrected
Map-model-unmasked
Map-model-masked
Fourier Shell Correlation
FSC=0.143
Spatial Frequency (1/Å)
Elevation
Azimuth
# of Images

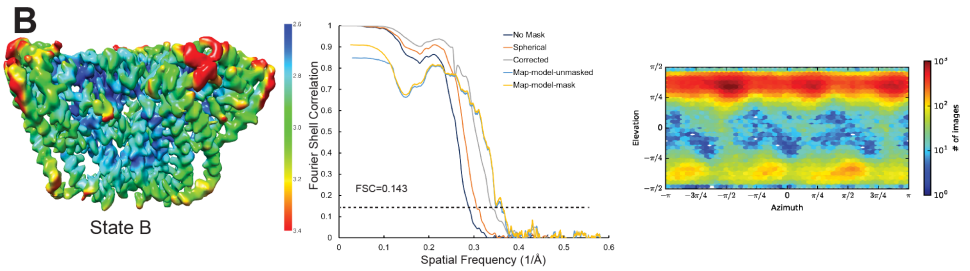
B
State B
No Mask
Spherical
Corrected
Map-model-unmasked
Map-model-mask
Fourier Shell Correlation
FSC=0.143
Spatial Frequency (1/Å)
Elevation
Azimuth
# of Images

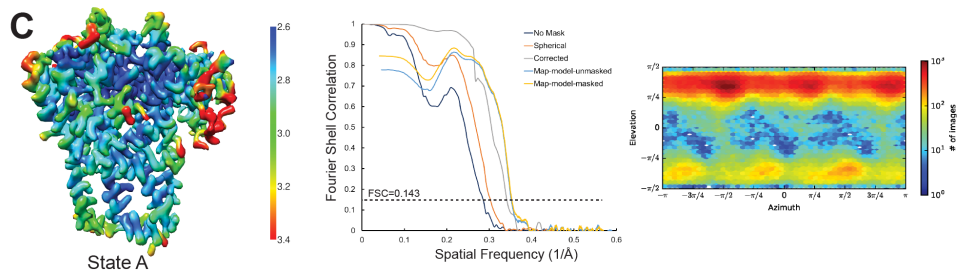
C
State A
No Mask
Spherical
Corrected
Map-model-unmasked
Map-model-masked
Fourier Shell Correlation
FSC=0.143
Spatial Frequency (1/Å)
Elevation
Azimuth
# of Images

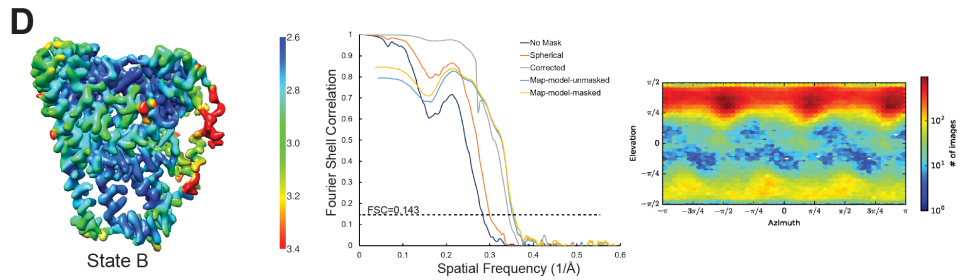
D
State B
No Mask
Spherical
Corrected
Map-model-unmasked
Map-model-masked
Fourier Shell Correlation
FSC=0.143
Spatial Frequency (1/Å)
Elevation
Azimuth
# of Images

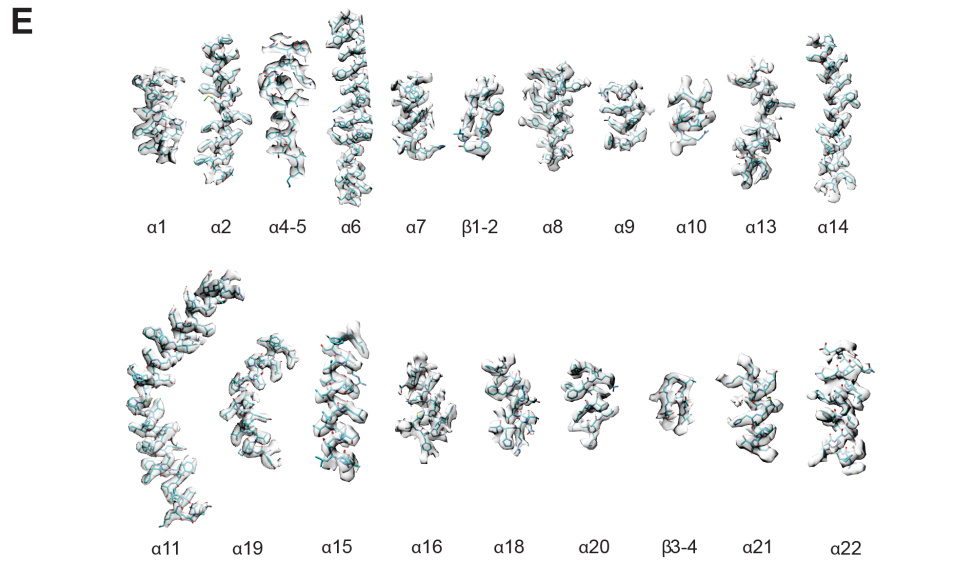
E
α1
α2
α4-5
α6
α7
β1-2
α8
α9
α10
α13
α14
α11
α19
α15
α16
α18
α20
β3-4
α21
α22

Figure S3. Resolution estimation of cryoEM 3D reconstructions of ATG9A, *Related to Figure 1*. **(A-D)** Local resolution maps (left panels), Fourier Shell Correlation (FSC) curves (middle panels) and orientation distribution plots (right panels) of the 3D reconstructions of ATG9A trimers (**A** and **B**) and "monomers" after density subtraction (**C** and **D**). Local resolution maps were generated by cryoSPARC2 and shown as surface. **E)** Refined coordinate model fit of all representative regions in the cryoEM density.

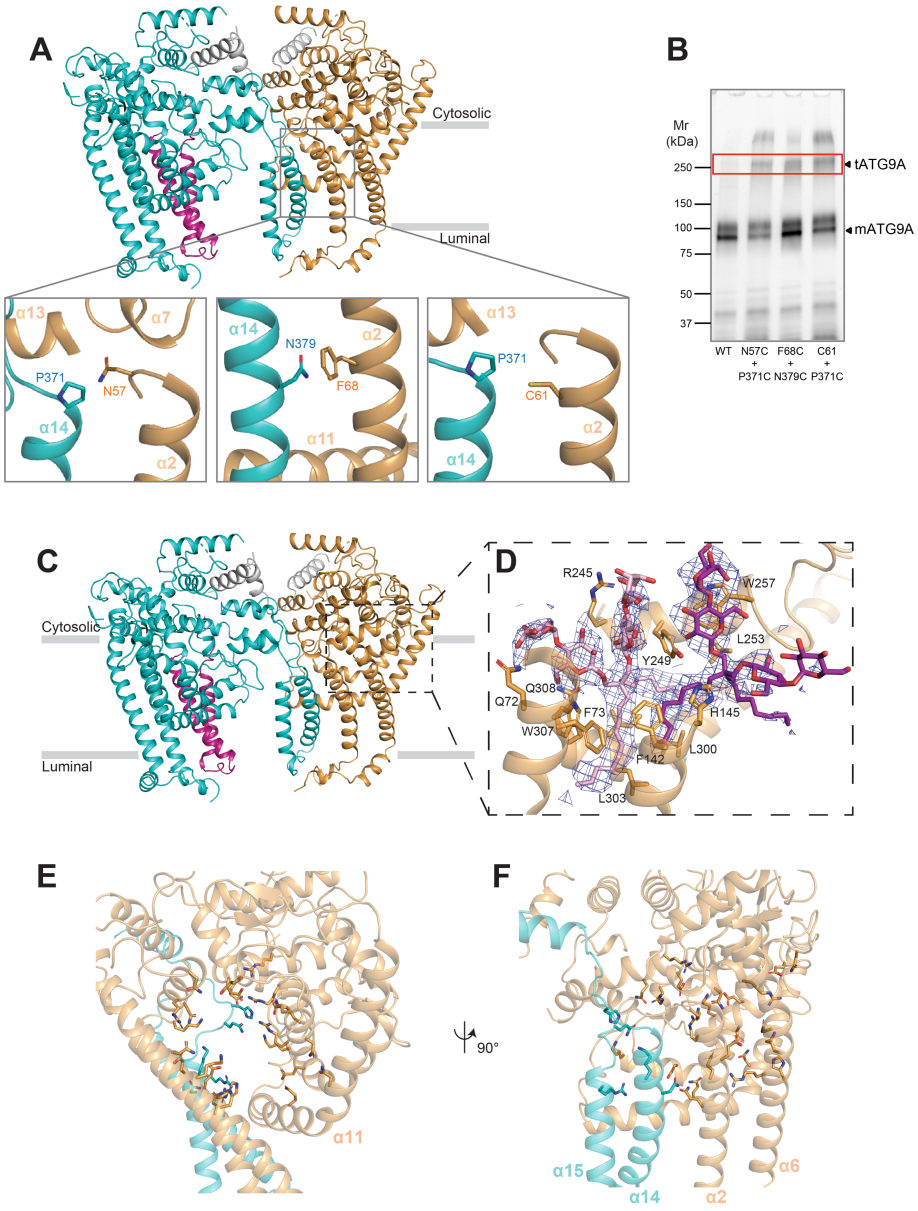

Figure S4. Trimerization of ATG9A validated by crosslinking, *Related to Figures 2,3 and 4.* (**A**) Location of the residues tested in crosslinking experiments shown in the structure of ATG9A in dark gray box. Close views of the mutated residues pairs are shown with lateral chains as sticks. The different protomer helices (α2 and α14) that define the greater part of the interface of trimerization are colored in cyan and orange. (**B**) SDS-PAGE analysis (using mVenus fluorescence) of ATG9A and selected mutants for crosslink formation after affinity purification in LMNG and treated with 10 mM DTT. The putative position of ATG9A trimer is shown with a red box. (**C**) ATG9A trimer with protomers colored, and edges of the membrane shown as gray thick lines. (**D**) Two bound LMNG molecules are colored pink and purple, and the main residues in the lateral branch interacting with the detergent molecules are shown as stick. Blue mesh represents for densities of LMNG. (**E,F**) Hydrophilic amino acid side chains lining the lateral branch of a protomer.

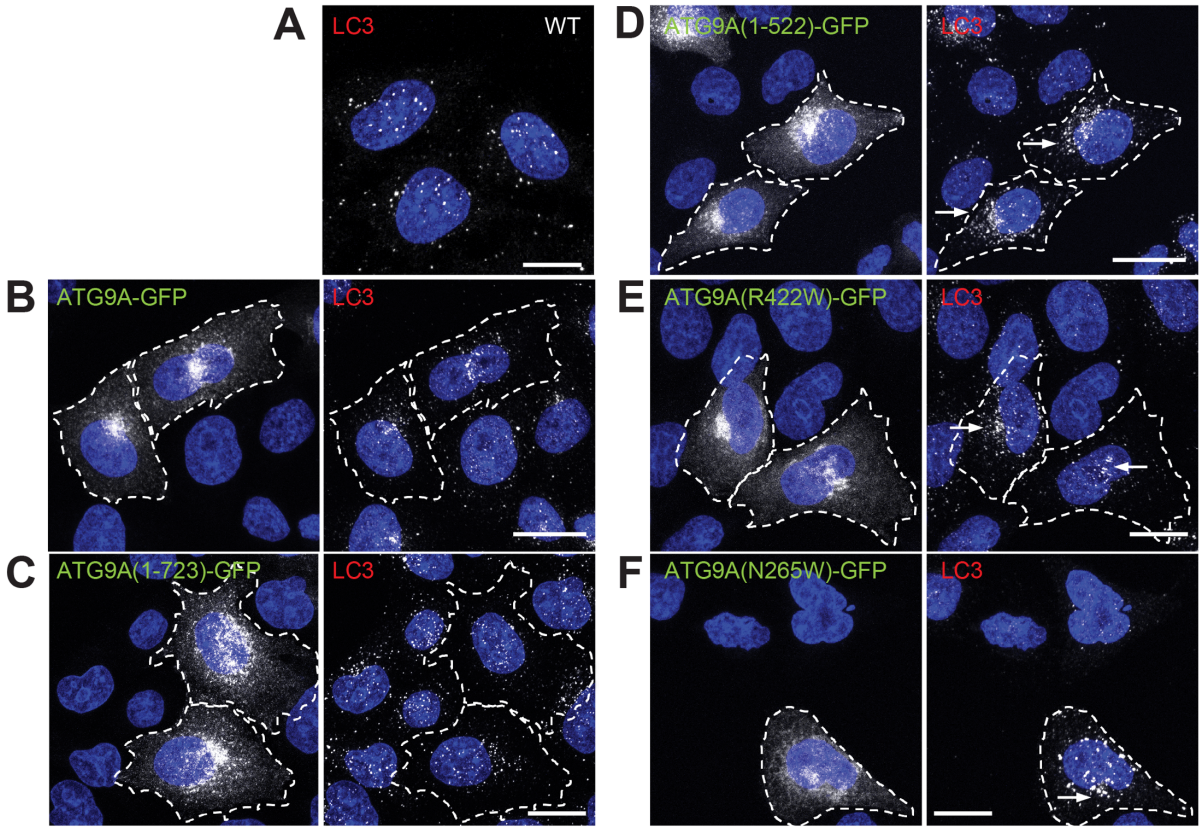

Figure S5. Dominant-negative effects of ATG9A constructs with deletion of the C-terminal domain or mutation of conserved residues in the central pore, *Related to Figure 5.* (**A**) Confocal microscopy of WT HeLa cells immunostained for endogenous LC3B. (**B-F**) WT HeLa cells were transfected with plasmids encoding various GFP-tagged ATG9A constructs (WT, 1-723, 1-522, R422W or N265W), and immunostained for endogenous LC3B. Transfected cells are indicated by the dashed outlines. Scale bar: 10 μm. Notice that full-length and 1-723 do not affect the distribution and size of LC3B puncta, but 1-522, R422W and N265W do, even in WT HeLa cells.

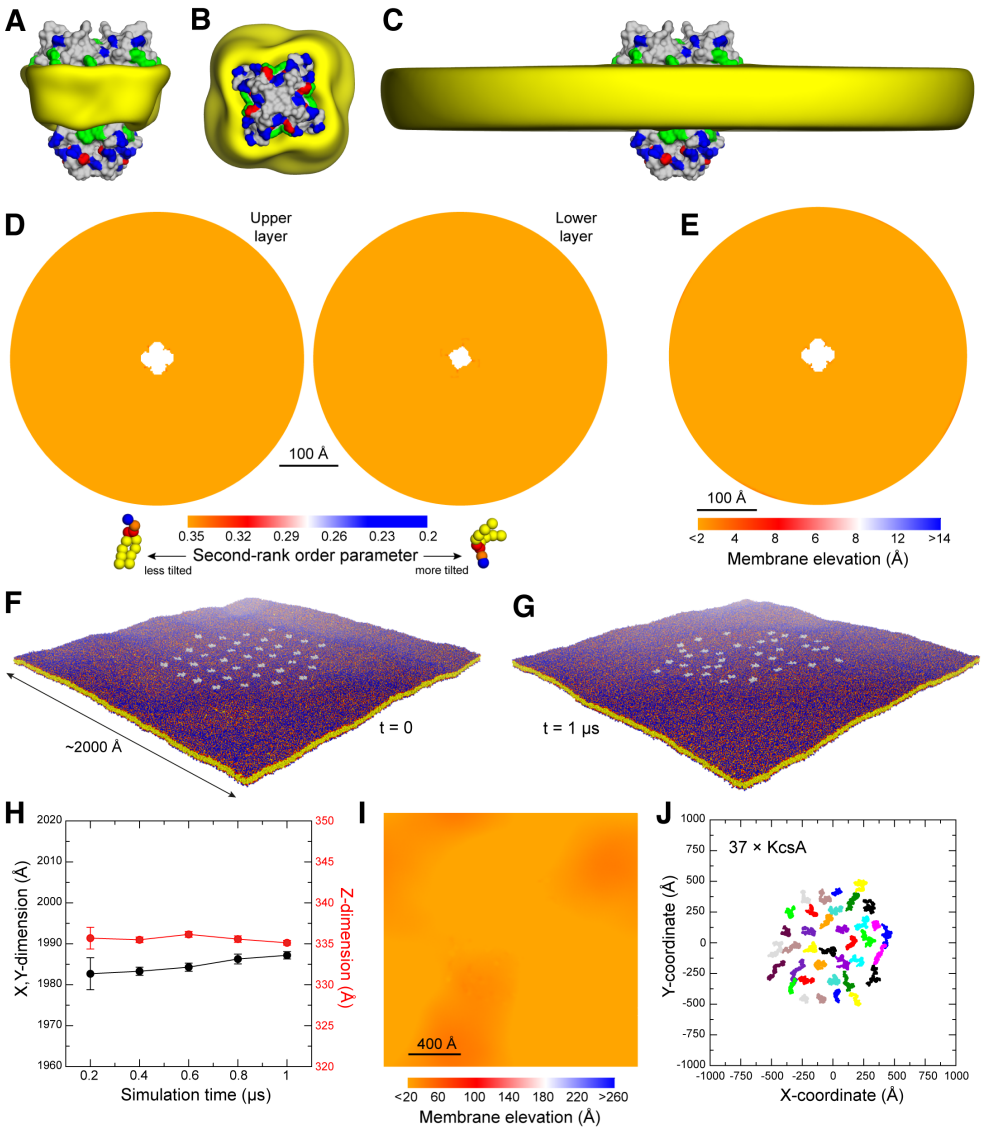

Figure S6. MD simulations of the K⁺ channel KcsA in a POPC bilayer, *Related to Figures 6 and 7.* (**A**) The protein is shown alongside a 3D density map (yellow) for the first shell of lipid-alkyl chains (*i.e.*, within 10 Å from the protein surface), calculated from the trajectory data. (**B**) Same as **A**, viewed from the cytoplasm. (**C**) Same as **A**, including lipid-alkyl chains within 100 Å from the protein surface. (**D**) Mean second-rank order parameter of the C-C bonds along the lipid alkyl chains, for either the outer or inner layers of the bilayer. See Figure 6F for more details and comparison with ATG9A. (**E**) Quantification of the perturbation of the membrane induced by KcsA. Shown is a map of the mean value of the Z-coordinate of the center of the bilayer, calculated from the trajectory data. The white space in the center corresponds to the area occupied by KcsA. Compare with Figure 6B. (**F, G**) View of the periodic unit cell used to simulate a cluster of KcsA proteins (gray) in a POPC lipid bilayer (colors), at the beginning and at the end of the calculated trajectory of 1 μs, respectively. (**H**) Time-evolution of the X,Y and Z dimensions of the simulation system shown in **F**. Compare with Figure 7E. (**I**) Quantification of the membrane perturbation induced by the cluster of KcsA proteins. Compare with Figure 7C. (**J**) Free lateral diffusion of the 37 copies of KcsA in the course of the calculated trajectory of 1 μs. Each trace (colors) represents the center-of-mass of one KcsA protein. Compare with Figure 7F.

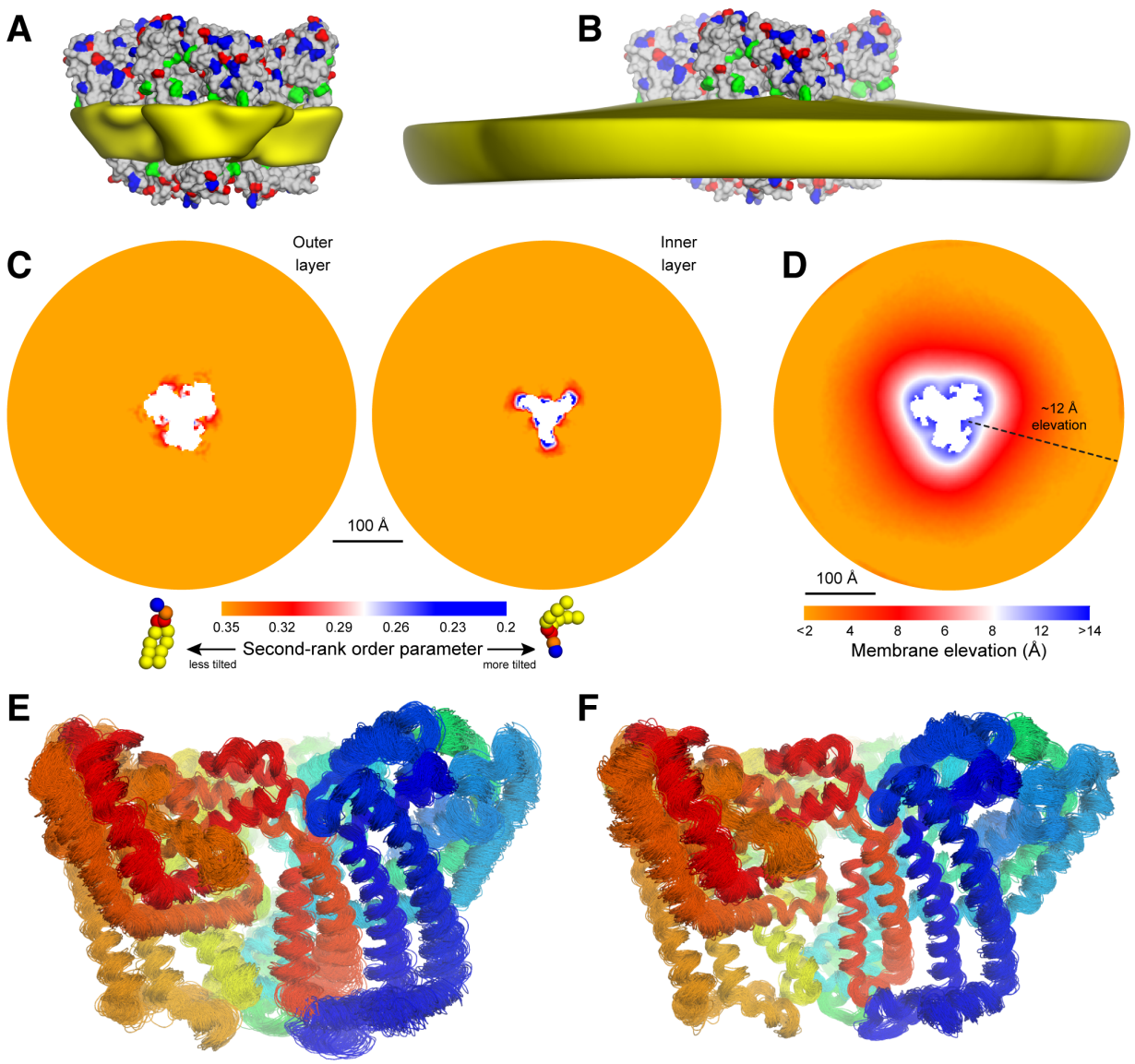

Figure S7. Molecular dynamics simulations of isolated ATG9A in a POPC bilayer, *Related to Figures 6 and 7.* The panels show data analogous to those included in Figure 6, for a simulation based on 'State A' rather than 'State B'. Consistent with the finding that the ATG9A protomers in 'State A' are slightly more upright relative to the membrane perpendicular, we observe that the second-rank lipid-order parameter values near the protein interface are slightly less shifted, relative to bulk values, when compared with 'State B'; the apex and range of the membrane deformation induced by the homotrimer are also only slightly reduced. (**E**) Overlay of 100 snapshots of the protein carbon-alpha trace, extracted from the simulated MD trajectory for 'State A', in 10-ns intervals. (**F**) Same as (E), for 'State B'.

Table S1. CryoEM data acquisition, image processing, and model refinement, *Related to Figure 1.*

Data collection and processing				
Magnification	130,000			
Voltage (kV)	300			
Exposure time (s/frame)	0.2			
Number of frames	50			
Electron exposure (e–/Å^2)	71			
Defocus range	-0.7 to -2.5			
Pixel size (Å)	1.06			
Symmetry imposed	C3 or C1			
	State A		State B	
	trimer	monomer	trimer	monomer
Initial particle images (no.)	6,926,538	1,781,160	6,926,538	1,938,873
Final particle images (no.)	593,720	290,672	646,291	341,231
Map resolution (Å)	2.8	2.9	2.9	2.9
FSC threshold	0.143	0.143	0.143	0.143
Refinement				
Non-hydrogen atoms	14128	5380	11955	5148
Protein residues	1715	653	1410	615
Ligands	6	2	6	2
R.m.s deviations				
Bond lengths (Å)	0.013	0.004	0.009	0.005
Bond angles (°)	1.732	0.708	1.341	0.738
Validation				
MolProbity score	2.79	1.99	2.35	1.83
Clashscore	22.35	9.09	9.08	8.49
Poor rotamers (%)	3.38	0	4.08	0
Ramachandran Plot				
Favored (%)	90.24	91.52	93.97	94.66
Allowed (%)	8.99	8.16	5.6	5.18
Disallowed (%)	0.77	0.31	0.43	0.17